



**HAL**  
open science

# A micromechanical muUNSAT effective stress expression for stress-strain behaviour of wet granular materials

Jérôme Duriez, R. Wan

## ► To cite this version:

Jérôme Duriez, R. Wan. A micromechanical muUNSAT effective stress expression for stress-strain behaviour of wet granular materials. *Geomechanics for Energy and the Environment*, 2018, 15, pp.10-18. 10.1016/j.gete.2017.12.003 . hal-01893074

**HAL Id: hal-01893074**

**<https://hal.science/hal-01893074v1>**

Submitted on 11 Oct 2018

**HAL** is a multi-disciplinary open access archive for the deposit and dissemination of scientific research documents, whether they are published or not. The documents may come from teaching and research institutions in France or abroad, or from public or private research centers.

L'archive ouverte pluridisciplinaire **HAL**, est destinée au dépôt et à la diffusion de documents scientifiques de niveau recherche, publiés ou non, émanant des établissements d'enseignement et de recherche français ou étrangers, des laboratoires publics ou privés.

## A micromechanical $\mu$ UNSAT effective stress expression for stress-strain behaviour of wet granular materials

J. Duriez<sup>a,b,\*</sup>, R. Wan<sup>a</sup>

<sup>a</sup>University of Calgary, Calgary, AB, T2N 1N4, Canada

<sup>b</sup>Irstea, UR RECOVER, F-13182 Aix-en-Provence, France

---

### Abstract

The definition of an effective stress variable for idealized triphasic granular media as the contact stress arising from interparticle forces is examined through discrete element modelling computations in concert with appropriately derived analytical stress expressions based on homogenization. The latter take a more practical importance, in that they also circumvent the need for direct measurements of interparticle contact forces. Considering dry or pendular-regime conditions for slightly polydisperse dense and loose packings, the contact stress-strain behaviours in dry or wet conditions are compared along a variety of loading paths, depending on the level of plastic dissipation involved. The contact stress indeed emerges as an effective stress variable with a remarkable stress-strain character along contractant loading paths and for dense solid packings where the behaviour is close to be non-dissipative. Along more dilatant loading paths or for looser packings, plastic dissipation increases and the coincidence of the constitutive behaviour in both dry and triphasic conditions is restricted to the initial stages of the loading paths, limiting the applicability of the contact stress to the estimation of initial stiffnesses. The stark constitutive differences between the proposed effective stress and Bishop's stress are also highlighted.

*Keywords:* effective stress, Discrete Element Method (DEM), granular, pendular,  $\mu$ UNSAT

---

\*Corresponding author

Email address: [jerome.duriez@irstea.fr](mailto:jerome.duriez@irstea.fr) (J. Duriez)

## 1. Introduction

Energy and Environmental Engineering operations require a precise mechanical description of multiphase porous media such as in oil and gas reservoirs, or partially water-saturated (unsaturated) soils. Obviously, the presence of various fluids within the pore space network of these multiphase materials greatly modifies their mechanical behaviour with respect to the dry (air-saturated) state which is well understood. For biphasic (or two-phase) porous media penetrated by a single pore fluid, a unified mechanical description by way of dry state constitutive models actually exists whatever the pore fluid and its pressure are following Terzaghi's and Biot's effective stress equations [1, 2]. Turning to triphasic (or three-phase) conditions with an immiscible fluid mixture, it would also be highly beneficial to extend this effective stress concept so that triphasic materials can be described by just inserting an adequate single effective stress into models designed for dry materials. In other words, the objective is to obtain a stress-strain-strength effective stress that would allow failure criterion and constitutive relations from dry conditions, all together, to be applied to triphasic conditions in order to easily predict limit stress states and strains. However, the exact determination of such a single effective stress has revealed to be highly challenging ever since the early Bishop's attempts [3].

When describing failure in triphasic media, it has been often possible to resort to an effective stress framework based on limit stress states according to dry shear strength criteria [4, 5, 6, 7, 8]. In these works, the effective stress is either phenomenologically deduced from Bishop's equation with appropriate expressions for  $\chi$  coefficient [4, 7], or as the contact forces stress contribution which can be indirectly accessed by subtracting a so-called suction stress from the total stress [5, 6, 8]. The suction stress [5] encompasses all relevant stress contributions in triphasic materials, excluding the contact stress stemming from the contact forces between the solid grains of the skeleton, and can be identified for granular materials with the capillary stress since other physico-chemical forces are then negligible. As for the contact stress, the latter appears as a

31 logical stress-strength effective stress since pore water is reported to have little  
32 or no influence onto the contact-scale local frictional threshold [9, 10], which  
33 thus leads to unique limit states for the macroscopic contact stress and a unified  
34 failure description irrespective of saturation.

35 Whereas in the biphasic case unique constitutive relations are related to  
36 strains via Biot’s effective stress, no effective stress has yet been found that  
37 would relate to strains in triphasic conditions through dry constitutive relations  
38 [7]. As such, the application of an effective stress principle to triphasic materials  
39 has often been challenged since Bishop himself [3], with alternate approaches  
40 relying on total stress and another stress variable such as matric suction to de-  
41 scribe unsaturated conditions using additional constitutive equations that are  
42 specific to these triphasic conditions [11, 12]. A compromise may, nevertheless,  
43 be found in that quasi-elastic behaviour, e.g. volume change along overconsoli-  
44 dated oedometric loadings, may still be described in triphasic conditions using an  
45 effective stress framework [4, 13, 14]. Recent micromechanical results by the au-  
46 thors [8, 15] suggest that the same contact stress also enjoys such a quasi-elastic  
47 strain-stress effective nature, in addition to its stress-strength character. This  
48 seems to be indeed coherent because granular material strains derive from solid  
49 particle relative displacements that relate to contact forces through a unique  
50 contact law, irrespective of saturation.

51 The present work aims to provide new evidences that demonstrate the stress-  
52 strain effective character of the contact stress in any regime showing small plastic  
53 dissipation by considering a wide range of loading paths which were absent from  
54 previous studies [8, 15].

55 It is further noted that direct measurements of contact forces and contact  
56 stresses are still beyond reach in triphasic materials in spite of a current research  
57 in the field [16]. To address this shortcoming, the present paper first recalls in  
58 Section 2 the  $\mu$ UNSAT expressions that enable one to indirectly access the con-  
59 tact stress through capillary stresses and the fluid phase microstructures, whose  
60 measurements appear to be more feasible thanks to e.g. computed tomography  
61 [17, 18]. For the purpose of the paper, the choice is actually made to con-

62 sider a Discrete Element Method (DEM) model for wet granular materials [19],  
 63 presented in Section 3, which allows both direct and indirect measurements of  
 64 the contact stress from a comprehensive description of the microstructure of all  
 65 solid and fluid phases, including interfaces. Numerical comparisons of dry-wet  
 66 behaviours for slightly polydisperse materials along various loading paths are  
 67 then presented in Section 4, validating the stress-strain effective nature of the  
 68 contact stress in regimes with small dissipation, and hence the present  $\mu$ UNSAT  
 69 effective stress expression. Section 5 finally evidences the fundamental differ-  
 70 ences in the pendular regime between the present  $\mu$ UNSAT effective stress and  
 71 Bishop’s stress, whose inapplicability to wet conditions is once again demon-  
 72 strated.

## 73 2. Micromechanical $\mu$ UNSAT effective stress expression

### 74 2.1. Total stress decomposition from micromechanics

75 The  $\mu$ UNSAT approach expresses the contact stress by isolating from the  
 76 macroscopic total stresses  $\Sigma$ , all microscopic stress contributions due to the  
 77 various phases and interfaces that encompass triphasic granular media. First,  
 78 the solid  $s$  and fluid ( $n, w$ ) bulk phases are considered with their corresponding  
 79 volumes  $V_s, V_n$  and  $V_w$ . Here,  $n$  stands for the non-wetting fluid, e.g. air,  
 80 whereas  $w$  refers to the wetting one, e.g. water. Additionally, all three interfaces  
 81  $S_{\alpha\beta}$ ,  $\alpha, \beta = n, s, w$  are as well included in the approach since the corresponding  
 82 surface tensions  $\gamma_{\alpha\beta}$  necessarily belong to the internal forces of the triphasic  
 83 material. As such, the total stresses are given as follows:

$$84 \quad \Sigma = \frac{1}{V} \left( \sum_{\alpha=n,s,w} \int_{V_\alpha} \sigma_\alpha dV + \sum_{\alpha,\beta=n,s,w} \int_{S_{\alpha\beta}} \pi_{\alpha\beta} dS \right) \quad (1)$$

85 In Eq. (1), the fluid stresses  $\sigma_\alpha$ ,  $\alpha = n, w$ , are directly given by the corre-  
 86 sponding pressures  $u_\alpha \delta$  with  $\delta$  as the identity tensor, whereas the solid stress  
 87  $\sigma_s$  can be classically expressed in terms of the tractions acting along the solid  
 88 particles surfaces  $S_p$  [20]. The surface stress tensors  $\pi_{\alpha\beta} = \gamma_{\alpha\beta} (\vec{n} \otimes \vec{n} - \delta)$ ,  
 89 with  $\vec{n}$  as the normal to  $S_{\alpha\beta}$ , finally describe the surface tension fields acting as  
 internal forces within any interface  $S_{\alpha\beta}$  [21, 22, 23, 24].

90 Algebraic manipulations applied to Eq. (1) lead to the following  $\mu$ UNSAT  
 91 decomposition of  $\Sigma$  into the contact stress  $\sigma^{cont}$  and the capillary stress  $\sigma^{cap}$ ,  
 92 to which the solid fluid surface tensions  $\gamma_{s\alpha}$  eventually do not contribute in the  
 93 case of rigid solid particles [20, 22, 24]:

$$\Sigma - u_n \delta = \sigma^{cont} + \sigma^{cap} \quad (2)$$

$$\sigma^{cont} = \frac{1}{V} \sum_c \vec{f}^c \otimes \vec{l} \quad (3)$$

$$\begin{aligned} \sigma^{cap} &= -\frac{1}{V} \left[ u_c \left( V_w \delta + \int_{S_{sw}} \vec{n} \otimes \vec{x} dS \right) \right. \\ &\quad \left. + \gamma_{nw} \left( \int_{S_{nw}} (\delta - \vec{n} \otimes \vec{n}) dS + \int_{\Gamma} \vec{\nu} \otimes \vec{x} dl \right) \right] \\ &= -\frac{1}{V} \left[ u_c (\boldsymbol{\mu}_{Vw} + \boldsymbol{\mu}_{Ssw}) + \gamma_{nw} (\boldsymbol{\mu}_{Snw} + \boldsymbol{\mu}_{\Gamma}) \right] \end{aligned} \quad (4)$$

94 Eq. (3) refers to the standard definition of the contact stress tensor  $\sigma^{cont}$   
 95 from the contact forces  $\vec{f}^c$  between solid particles, and the corresponding branch  
 96 vector  $\vec{l}$  connecting the centroids of contacting particles.

97 In Eq. (4), the capillary stress  $\sigma^{cap}$  encompasses the remainder of the in-  
 98 ternal forces that arise both from the fluid-fluid surface tension  $\gamma_{nw}$  and the  
 99 capillary pressure  $u_c = u_n - u_w$  that is equal to suction in granular materials.  
 100 Four microstructure tensors  $\boldsymbol{\mu}_X$  reflect the tensorial nature of these internal  
 101 forces, with  $\boldsymbol{\mu}_{Vw}$  the only one being always spherical since it corresponds to  
 102 the isotropic action of suction within  $V_w$ . Other microstructure tensors have  
 103 a general, non-spherical, tensorial expression with e.g.  $\boldsymbol{\mu}_{Ssw}$  depending on the  
 104 orientation of the wetted surface  $S_{sw}$  since the latter sustains suction along its  
 105 normal only. Also,  $\boldsymbol{\mu}_{Snw}$ ,  $\boldsymbol{\mu}_{\Gamma}$  reflect the orientations of the interface  $S_{nw}$  and of  
 106 the three-phase contact lines  $\Gamma$  that are subjected to fluid-fluid surface tension,  
 107 where  $\vec{\nu}$  in Eq. (4) is the tangent to  $S_{nw}$  being normal to  $\Gamma$  [20].

## 108 2.2. $\mu$ UNSAT contact stress expression

109 Isolating  $\sigma^{cont}$  in Eq. (2)-(4), the following  $\mu$ UNSAT expression for the  
 110 contact stress is eventually obtained:

$$\sigma^{cont} = \Sigma - u_n \delta + \frac{1}{V} \left[ u_c (\boldsymbol{\mu}_{Vw} + \boldsymbol{\mu}_{Ssw}) + \gamma_{nw} (\boldsymbol{\mu}_{Snw} + \boldsymbol{\mu}_{\Gamma}) \right] \quad (5)$$

111 Such an expression is believed to provide an easier access to  $\sigma^{cont}$  during ex-  
 112 periments than the direct definition of Eq. (3). Imaging techniques such as  
 113 computed tomography indeed are very promising in allowing precise measure-  
 114 ments of the fluid phase microstructures [17, 18]. Then, one would be able  
 115 to compute the microstructure tensors  $\mu_{\mathbf{x}}$  in Eq. (5), as opposed to requiring  
 116 more complex contact force measurements [16] that enter the direct contact  
 117 stress expression, Eq. (3).

118 Leaving any experimental endeavour aside for now, Eq. (5) is herein used  
 119 within the framework of DEM to investigate the very role of the contact stress  
 120 in connection with strains, and whether it may serve as a strain-stress-strength  
 121 effective stress expression.

### 122 3. DEM multiscale modelling of triphasic granular materials

123 Numerical DEM models indeed provide a convenient multiscale description  
 124 of triphasic granular materials whereby the microstructure of all solid and fluid  
 125 phases is easily measured. As such, the contact stress can be readily estimated  
 126 using either Eq. (3) or (5) along various loading paths and for different packings.

#### 127 3.1. Model formulation

128 Previously proposed in [19] and implemented in the Yade code [25], the  
 129 considered DEM model addresses the case of spherical solid particles and a  
 130 wetting fluid distribution in terms of distinct capillary bridges, i.e. menisci be-  
 131 tween particles pairs (Fig. 1), in accordance with the so-called pendular regime,  
 132 also referred to as wet conditions. Such conditions correspond to a low wetting  
 133 saturation,  $S_w$ , only, where  $S_w$  is defined as:

$$S_w = \frac{V_w}{V_w + V_n} \quad (6)$$

134

135 In line with another DEM approach [26], the model does not compute any  
 136 biphasic pore flow, but instead assumes thermodynamic equilibrium and uni-  
 137 form capillary pressure conditions. As such, the menisci properties are computed

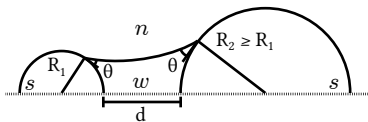


Figure 1: A capillary bridge

138 from the following Laplace-Young equation (7) which relates capillary pressure  
 139 to surface tension and the interface curvature  $\text{div}(\vec{n})$ , with  $\vec{n}$  being the normal  
 140 to  $S_{nw}$  pointing from  $n$  to  $w$ :

$$u_c = \gamma_{nw} \text{div}(\vec{n}) \quad (7)$$

141 According to the thermodynamic equilibrium assumption, Eq. (7) is solved  
 142 for uniform values of  $u_c$  throughout the sample, also considering a uniform and  
 143 constant contact angle  $\theta$  (Fig. 1) [19]. As discussed in greater depth in [19],  
 144 Eq. (7) is actually solved depending on the particles radii and their distance, in  
 145 addition to imposed  $u_c$  and  $\theta$ . Based on the  $S_{nw}$  interface profile, the numerical  
 146 solution procedure finally outputs the resultant capillary force  $\vec{f}^{cap}$  and other  
 147 relevant microstructural quantities such as  $\mu_{S_{nw}} = \int_{S_{nw}} (\delta - \vec{n} \otimes \vec{n}) dS$  for  
 148 instance, thus enabling one to apply the  $\mu$ UNSAT Eq. (5) and measure contact  
 149 stresses during DEM simulations [19].

150 The model actually inserts capillary bridges at each new contact between  
 151 solid particles, with properties given by the Laplace-Young equation. In the  
 152 instance the particles subsequently separate, the capillary bridge remains until  
 153 some limit distance beyond which the Laplace-Young equation does not yield  
 154 any solution. This hysteretic mechanism of bridge formation and rupture is  
 155 consistent with experimental observations [27] and occurs in the model in a  
 156 fully drained manner. The presence of a capillary bridge between two particles  
 157 corresponds to a capillary interaction with the corresponding attractive capillary  
 158 force  $\vec{f}^{cap}$  due to the capillary pressure and surface tension loadings along the  
 159 wetted surfaces  $S_{sw}$  and the contact lines  $\Gamma$ .

160 In addition, the interaction between touching particles is governed by clas-  
 161 sical elastic-plastic frictional (cohesionless) contact laws whereby normal and



162 tangential relative displacements between particles are restricted by normal and  
 163 tangential contact forces  $f_n^c$  and  $f_t^c$  [8, 19]. A simplified linear elastic behaviour  
 164 of the contact interaction is first defined by the normal and tangential local  
 165 stiffnesses,  $k_n$  and  $k_t$ , which are directly obtained from the average diameter  $\bar{D}$   
 166 of any pair of contacting particles and the model parameters  $k_n/\bar{D}$  and  $k_t/k_n$ :

$$k_n = \frac{k_n}{\bar{D}} \bar{D} \quad (8)$$

$$k_t = \frac{k_t}{k_n} k_n \quad (9)$$

167 with the consideration of an elastic shear stiffness being eventually restricted by  
 168 the following Coulombian friction threshold, with  $\mu$  the friction coefficient:

$$|f_t^c| \leq \mu f_n^c \quad (10)$$

169 Table 1 lists all parameters of the DEM model. The retained values for the  
 170 contact interaction parameters,  $k_n/\bar{D}$  and  $k_t/k_n$ , are similar to previous studies  
 171 [8, 24, 19, 20]. As for the capillary interaction, the latter is fully determined  
 172 by the fluid-fluid surface tension  $\gamma_{nw}$ , the contact angle  $\theta$  and the particle size  
 173 distribution. Air-water surface tension at ambient temperature is considered for  
 174  $\gamma_{nw}$  while a low though not zero  $\theta$ -value corresponds to the wetting of glass beads  
 175 by water, having at the same time the convenience of enhancing the mechanical  
 176 effects of triphasic conditions [19]. Finally, silt-like particle diameters are chosen  
 177 with a narrow particle size distribution being uniform in number between  $D_{min}$   
 178 and  $D_{max}$ .

Contact			Capillarity		Packing	
$k_n/\bar{D}$	$k_t/k_n$	$\mu$	$\gamma_{nw}$	$\theta$	$D_{min}$	$D_{max}$
(MPa)	(-)	(-)	(N/m)	(°)	( $\mu\text{m}$ )	( $\mu\text{m}$ )
10	0.5	0.5	0.073	10	21	25

Table 1: DEM model parameters

179 While the dynamic scheme of the DEM is classically carried out using some  
 180 numerical damping, in order to obtain more easily a quasi-static evolution of the  
 181 system, the damping coefficient [25] is taken as low as 0.05 to avoid numerical

182 artifacts. Quasi-staticity is systematically verified through low values of the  
 183 particle unbalanced forces [25] which were below 1% during all loading cases.  
 184 As such, particle inertia (mass) does not play any role in the computations,  
 185 which allows the use of density scaling with an artificially high density value  
 186 ( $\rho = 20,000 \text{ kg/m}^3$  instead of  $2,600 \text{ kg/m}^3$ ) for the particles. Without any  
 187 consequence on the quasi-static rheology, density scaling reduces computational  
 188 costs through larger time steps, even though loading rates have to be marginally  
 189 reduced for quasi-staticity to still hold.

190 The DEM sample is a parallelepiped, initially a cube approximately 0.6 mm a  
 191 side depending on packing density, with 6 rigid walls that enclose a total number  
 192 of 20,000 spherical Discrete Elements (DE). Similar numbers (10,000 to 20,000)  
 193 are classically used in material-scale DEM analyses [26, 19, 20, 28] in order to  
 194 avoid numerical result dispersion from one numerical sample to another as well  
 195 as field heterogeneity, in conformity with the Representative Elementary Volume  
 196 (REV) concept. The DE sample is packed at various levels to produce different  
 197 states in density as quantified by the porosity  $n$  and the average coordination  
 198 number  $z_c$ :

$$n = \frac{V_n + V_w}{V_s + V_n + V_w} = \frac{V_v}{V} \quad (11)$$

$$z_c = \frac{2 N_c - N_1}{N_p - N_1 - N_0} \quad (12)$$

199 with  $N_c$  the total number of contacts, and  $N_0 + N_1$  the number of excluded  
 200 rattlers, i.e. particles with zero or only one contact, and  $N_p$  the total number of  
 201 DE. All considered packings are initially isotropic and prepared such that dry  
 202 vs wet comparisons can be conducted in an unbiased manner.

203 Care is indeed taken in considering dry or wet solid packings to be compara-  
 204 ble in terms of  $n$  and  $z_c$  as these parameters obviously affect the dry constitutive  
 205 relation which should also be described in wet conditions by an effective stress.  
 206 As such, an appropriate particle packing generation procedure is followed which  
 207 first involves a classical isotropic compression until a desired confining pressure  
 208 is reached to obtain dense or loose dry packings [26], without the consideration  
 209 of any capillary interaction that is only introduced in a second stage for the

210 wet samples. In this manner, wet packings show initial states which are barely  
 211 affected by the presence of capillary forces, and thus compare well with dry  
 212 packings.

### 213 3.2. Dry and wet strain proportional loading paths

214 In order to investigate the stress-strain effective nature of the contact stress,  
 215 the DEM model is used to explore the existence of a unique constitutive relation  
 216  $\mathcal{F}$  between  $\boldsymbol{\sigma}^{cont}$  and the strains  $\boldsymbol{\varepsilon}$  in both dry (biphasic) and wet (triphasic)  
 217 conditions. In the case of such an existence,  $\mathcal{F}$  by definition would relate the  
 218 current contact stress  $\boldsymbol{\sigma}^{cont}(t)$  to the strain loading path  $[\boldsymbol{\varepsilon}(\tau); -\infty < \tau \leq t]$   
 219 such that:

$$\boldsymbol{\sigma}^{cont}(t) = \mathcal{F}([\boldsymbol{\varepsilon}(\tau); -\infty < \tau \leq t]) \quad (13)$$

220 Extending our previous work [8, 15] where classical triaxial paths were exam-  
 221 ined, the validity of the same Eq. (13) in dry and wet conditions with a unique  
 222  $\mathcal{F}$  is herein probed considering axisymmetric strain proportional loading paths,  
 223 with ‘1’ as the axis of symmetry and ‘2, 3’ the two other spatial directions:

$$d\varepsilon_1 = cst \geq 0 ; d\varepsilon_2 = d\varepsilon_3 ; d\varepsilon_1 + 2Rd\varepsilon_3 = 0 \quad (14)$$

224 The loading parameter  $R \geq 0$  is constant along a given path,  $R = 1$  corresponds  
 225 to an isochoric loading path, whereas dilatancy (resp. contractancy) is imposed  
 226 for  $0 < R < 1$  (resp.  $R > 1$ ). The limiting case  $R = 0$  is defined as another  
 227 contractant path ( $d\varepsilon_1 = 0 ; d\varepsilon_2 = d\varepsilon_3 = cst \geq 0$ ).

228 Let’s denote the volumetric strain as  $\varepsilon_V$ :

$$\varepsilon_V = \varepsilon_1 + 2\varepsilon_3 \quad (15)$$

229 and choose  $\|\boldsymbol{\varepsilon}\|$  (the Euclidean norm of  $\boldsymbol{\varepsilon}$ ) as a monotonously increasing loading  
 230 parameter, i.e.

$$\|\boldsymbol{\varepsilon}\| = \sqrt{\varepsilon_1^2 + 2\varepsilon_3^2} \quad (16)$$

231 Accordingly, Fig. 2 illustrates the corresponding dilatancy rates of four loading  
 232 paths with  $R \in \{0; 0.2; 1; 5\}$  that will be considered in the following analysis. In  
 233 all cases, imposed strain rates are low enough to ensure quasi-static simulations

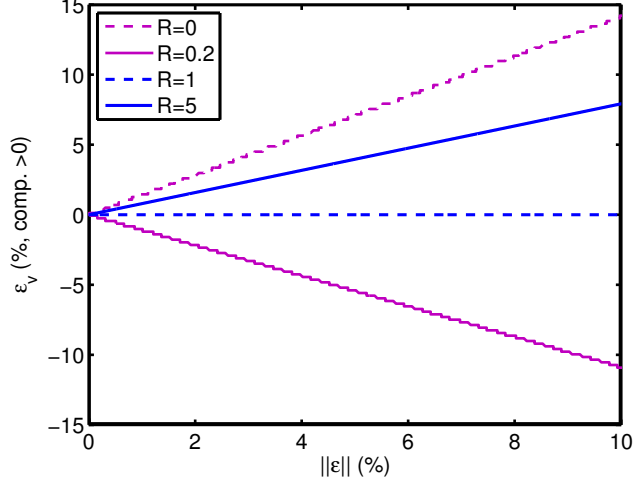


Figure 2: Dilatancy rates of imposed loading paths for  $R \in \{0; 0.2; 1; 5\}$

234 as verified from the corresponding low values of the particle unbalanced forces  
 235 [25] which were below 1%.

236 The main objective of imposing such strain loading paths on both dry and  
 237 wet packings is to verify the hypothesis,  $\boldsymbol{\sigma}' = \boldsymbol{\sigma}^{cont}$ , upon which is founded  
 238 the  $\mu$ UNSAT framework. If Eq. (13) holds, then the resulting contact stress  
 239 paths should coincide in both dry and wet conditions. Recognizing the axial  
 240 symmetry of the problem, it is convenient to associate the tensor  $\boldsymbol{\sigma}^{cont}$  with  
 241 the two classical scalars (invariants)  $p^{cont}$  and  $q^{cont}$ , i.e.

$$p^{cont} = \frac{\sigma_1^{cont} + 2\sigma_3^{cont}}{3} \quad (17)$$

$$q^{cont} = \sigma_1^{cont} - \sigma_3^{cont} \quad (18)$$

242 while similarly,  $p$  and  $q$  variables pertain to the total stress tensor  $\boldsymbol{\Sigma}$ :

$$p = \frac{\Sigma_1 + 2\Sigma_3}{3} \quad (19)$$

$$q = \Sigma_1 - \Sigma_3 \quad (20)$$

243 **4. Validity of the  $\mu$ UNSAT effective stress**

244 *4.1. Dense packings*

245 Proportional strain loading paths are first imposed to dense solid packings.  
 246 In essence, the same strain loading path is imposed to similarly dense packings  
 247 in both dry and wet conditions with the resulting contact stress paths recorded.  
 248 The contact stress obviously coincides with the total stress in dry conditions,  
 249 whereas Eq. (3) or (5) can be indistinctly used to access the contact stress under  
 250 wet conditions [28].

251 Four strain loading paths are considered with  $R \in \{0; 0.2; 1; 5\}$ , under two  
 252 different confining pressures referred to as “A” and “B”. For each confining  
 253 pressure A or B, and each  $R$  value, one dry and one wet test are considered,  
 254 leading to 16 tests on dense packings in total. Table 2 gives details of the initial  
 255 conditions for the dry-wet test pairs A, B pertaining to dense packings. These  
 256 initial conditions are such that dry and wet tests of a given pair A or B show  
 257 initial states  $(\sigma^{cont}, n, z_c)$  being as close as possible.

	Tests A		Tests B	
	Dry	Wet	Dry	Wet
Initial $p$ (kPa)	11.1	2	20.6	10
Imposed $u_c$ (kPa)	—	25	—	125
Initial $S_w$ (%)	—	7.18	—	0.85
Initial $n$ (-)	0.375	0.380	0.370	0.373
Initial $z_c$ (-)	6.41	6.21	6.62	6.52

Table 2: Tests data for the dry and wet loading paths imposed on dense packings

258 Comparing the contact stress responses in dry and wet conditions (Fig. 3  
 259 and 4), it is indeed verified that virtually unique behaviours are observed along  
 260 the contractant or isochoric loading paths  $R \in \{0; 1; 5\}$ . As such, this establishes  
 261 the validity of using the dry constitutive relation  $\mathcal{F}$  together with  $\sigma^{cont}$  as an  
 262 effective stress along these loading paths.

263 As for the dilatant loading path  $R = 0.2$ , a unique behaviour is observed in  
 264 the early stage of the test. Subsequently, the imposed dilatancy rate requires the  
 265 stresses to eventually vanish in the dry case, whereas when wet the same packing

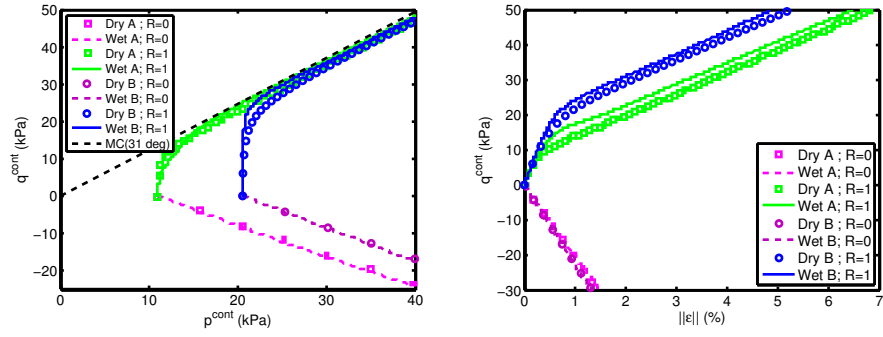


Figure 3: Contact stress response of a dense packing (Table 2) along contractant ( $R = 0$ ) and isochoric ( $R = 1$ ) strain loading paths (color version online)

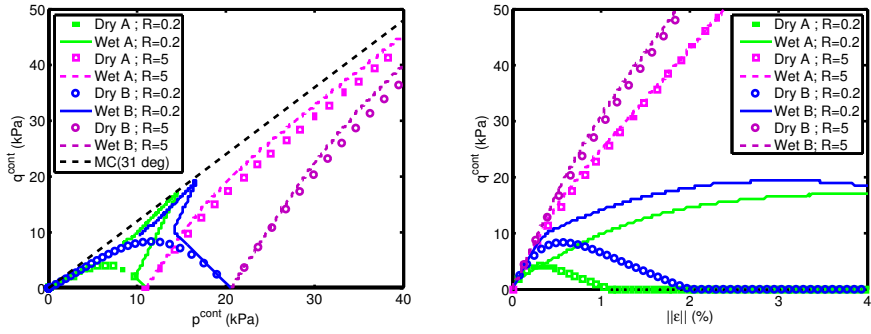


Figure 4: Contact stress response of a dense packing (Table 2) along contractant ( $R = 5$ ) and dilatant ( $R = 0.2$ ) strain loading paths (color version online)

266 gains a propensity to dilate originating from liquid bridges, thus avoiding a loss  
 267 in bearing capacity. Hence, for such a dilatant loading path, the role of the  
 268 contact stress as an effective stress is limited to the initial part of the loading  
 269 path, and could still be used to predict initial stiffnesses in triphasic conditions.

270 It is noted that all contact stress responses obtained in both dry and triphasic  
 271 conditions are found to be bounded by the same cohesionless Mohr-Coulomb  
 272 failure criterion (with  $c = 0$  Pa ;  $\varphi = 31^\circ$ ) that was previously measured in  
 273 dry conditions for such packings [15]. The universal property of this limit stress  
 274 line, irrespective of the phase condition, is another illustration of the previously  
 275 mentioned stress-strength effective nature of the contact stress.

#### 276 4.2. Loose packing

277 The same analysis procedure is now applied to loose packings (Table 3). The  
 278 numerical results displayed in Figs. 5 and 6 reveal less of an agreement between  
 279 dry and wet behaviours in comparison to the previous dense case study.

	Tests A		Tests B	
	Dry	Wet	Dry	Wet
Initial $p$ (kPa)	8.1	2	17.3	10
Imposed $u_c$ (kPa)	—	25	—	125
Initial $S_w$ (%)	—	4.17	—	0.50
Initial $n$ (-)	0.442	0.441	0.436	0.438
Initial $z_c$ (-)	4.96	4.84	5.17	5.12

Table 3: Tests data for the dry and wet loading paths imposed on loose packings

280 In particular, the existence of a unique constitutive relation  $\mathcal{F}$  between  $\sigma^{cont}$   
 281 and  $\varepsilon$  is identified for the most contractant loading path  $R = 0$  only, and is  
 282 somewhat approximated along the less contractant path  $R = 5$ .

283 As for the isochoric path  $R = 1$ , and at variance with the dense packing  
 284 (Fig. 3), a dry-wet agreement is only obtained for the very initial phase during  
 285 which  $p^{cont}$  remains constant, consistent with a possible relationship between  
 286  $\sigma^{cont}$  and  $\varepsilon$  through Hooke's elastic law. Then, the dry packing presents a  
 287 'liquefaction' behaviour with vanishing stresses, consistent with the constant  
 288 volume condition and the underlying material contractant flow rule. In contrast,

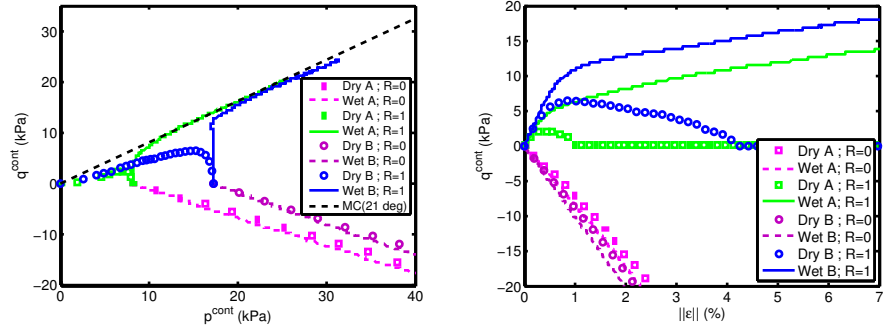


Figure 5: Contact stress response of a loose packing (Table 3) along contractant ( $R = 0$ ) and isochoric ( $R = 1$ ) strain loading paths (color version online)

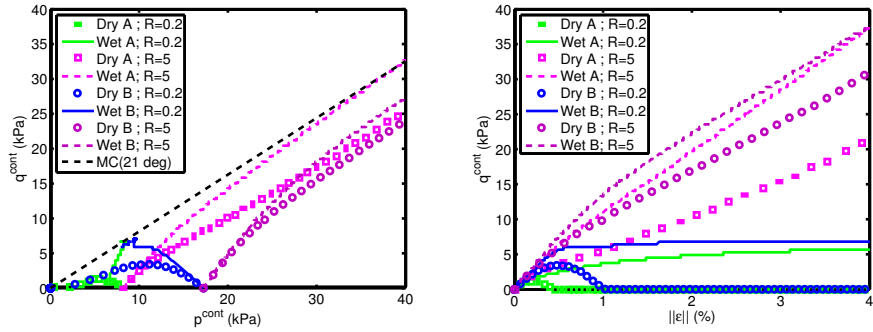


Figure 6: Contact stress response of a loose packing (Table 3) along contractant ( $R = 5$ ) and dilatant ( $R = 0.2$ ) strain loading paths (color version online)



289 similar packings under triphasic conditions gain a propensity to dilate due to  
 290 liquid bridges, thus leading the mean contact stress to increase.

291 Some influence of the mean contact stress on the dry-wet comparison is  
 292 finally observed along the dilatant loading path  $R = 0.2$ . Along such a path,  
 293 dry conditions induce the stresses in this loose material to vanish as expected,  
 294 while triphasic conditions enhance again the material dilatant nature, leading  
 295 to non zero stress states. The exact behaviour of the wet material nevertheless  
 296 depends on the confining pressure.

297 For a low confining pressure, the wet loose packing behaves similarly to the  
 298 dense one because capillary stress plays an important part of the total stresses:  
 299  $|p^{cap}|/p \approx 3.0$  and  $|p^{cap}|/p^{cont} \approx 0.75$  at the initial stage of this test. The  
 300 behaviour then changes into one with a greater propensity to dilate as a result  
 301 of triphasic conditions.

302 On the other hand, upon increasing the confining pressure, the contact  
 303 stress also increases while the capillary stress remains fairly constant, leading  
 304 to  $|p^{cap}|/p^{cont} \approx 0.42$  and  $|p^{cap}|/p \approx 0.72$ , initially. The changes in the rela-  
 305 tive contributions from contact and capillary stresses diminish the liquid bridge  
 306 induced dilatancy in the loose packing.

307 Finally, and as previously noted for the dense packing, the plastic limit  
 308 criterion ( $c = 0$  Pa ;  $\varphi = 21^\circ$ ) corresponding to this loose material under dry  
 309 conditions [15] also applies to the contact stress under triphasic conditions, once  
 310 again confirming the stress-strength effective nature of  $\sigma^{cont}$ .

### 311 4.3. Discussion: effective stress vs dissipation and elasticity

312 The influences of the loading path and the solid packing on the ability of  
 313  $\sigma^{cont}$  to act as a stress-strain effective stress are now interpreted in relation to  
 314 the variable dissipation associated with the observed behaviours. From  $f_n^c$  and  
 315  $f_t^c$  the normal and tangential components of the contact forces  $\vec{f}^c$ , the specific  
 316 elastic energy  $e^{el}$  of the material is:

$$e^{el} = \frac{1}{2V} \sum_{N_c} \left( \frac{(f_n^c)^2}{k_n} + \frac{(f_t^c)^2}{k_t} \right) \quad (21)$$

317 which is easily measured from the DEM model, together with its increment  
 318  $\delta e^{el}$  between successive states. Comparing this increment with the incremental  
 319 external work  $\Sigma : d\boldsymbol{\varepsilon}$ , the following quantity  $\lambda$  quantifies the deviation of the  
 320 mechanical behaviour of any dry test from a non-dissipative behaviour:

$$\lambda = \left| \frac{\Sigma : d\boldsymbol{\varepsilon} - \delta e^{el}}{\Sigma : d\boldsymbol{\varepsilon}} \right| \quad (22)$$

321 The quasi-static nature of the loading paths ensures that both the kinetic energy  
 322 and the energy term associated to numerical damping are negligible, and thus  
 323 do not contribute to the energy balance quantified by the quantity  $\lambda$ . As such,  
 324 during a non-dissipative, e.g. elastic, dry loading path,  $\lambda$  is equal to 0 throughout  
 325 since all external work is completely stored as elastic energy. On the other hand,  
 326 increasing values of  $\lambda$  reveal an increasing dissipation. It is noted that  $\lambda$  may  
 327 be greater than 1 in the instance of elastic energy loss ( $\delta e^{el} < 0$ ).

328 However, it is to stress out that a non-dissipative behaviour with negligi-  
 329 ble values of  $\lambda$  does not necessarily correspond to a stress-strain path being  
 330 reversible, even though the opposite is true. These intricacies are specific to  
 331 granular materials whose elastic energy is contained in a contact network whose  
 332 properties (for instance,  $N_c$  in Eq. (21)) fundamentally depend on irreversible  
 333 strains. Also, granular materials are prone to irreversible yet non-dissipative  
 334 local mechanisms such as contact losses. These very specific features can be  
 335 interpreted in terms of a locked elastic energy concept [29] and have also been  
 336 widely commented, e.g. in [30, 31], motivating here the distinction between the  
 337 “non-dissipative” and “elastic” terminologies.

338 From the evolutions of  $\lambda$  shown in Figs. 7, and comparing with previous  
 339 Figs. 3, it clearly appears that it is along the less dissipative loading paths that  
 340 the stress-strain effective nature of  $\boldsymbol{\sigma}^{cont}$  is the most marked, e.g.  $R = 0$ . Such  
 341 a result includes and extends the finding previously reported in [4, 13] that an  
 342 effective stress approach is possible in the elastic regime.

343 Another illustration of the role of dissipation in the effective stress discus-  
 344 sion is proposed in Fig. 8 which considers an extreme case of the DEM model,  
 345 referred to as  $\mu = \infty$ . In this extreme case of the DEM model, an ideal contact

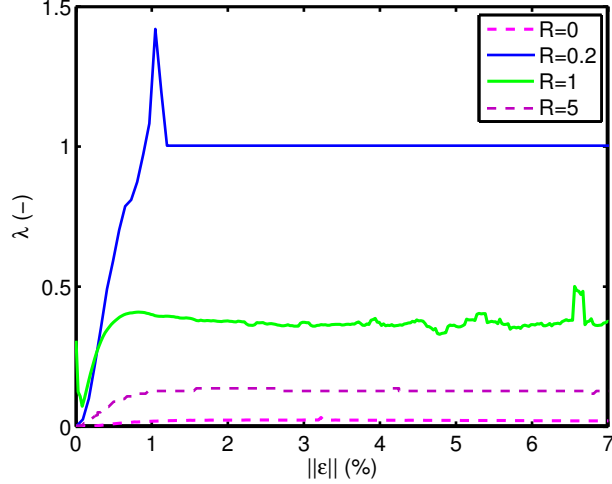


Figure 7: Dissipative nature of the behaviour during various dry loading paths imposed on the dense packing (Tests A). Raw data have been smoothed without altering the average trends and  $\lambda$ -values for  $R=0.2$  may be disregarded beyond  $\|\epsilon\| \approx 1\%$  since stresses vanish at this point

346 description is adopted in which no frictional threshold (10) limit is imposed on  
 347 the shear contact force:  $f_t^c$  just evolves linearly with the tangential relative dis-  
 348 placement according to the shear stiffness  $k_t$  as long as a contact exists. The  
 349 dry-wet comparisons shown in Fig. 8 then reveal an enhanced stress-strain effec-  
 350 tive character of  $\sigma^{cont}$  with this model, as opposed to the already discussed  
 351 dry-wet comparisons with the classical friction coefficient  $\mu = 0.5$  for the loose  
 352 packing along the  $R = 5$  loading path.

353 The present discussion finally sheds some light on the generality of ther-  
 354 momechanical approaches to effective stress, as proposed e.g. in [23, 32, 33].  
 355 Because the effective stress discussion herein appears to be widely different de-  
 356 pending on the elastic or dissipative nature of the behaviour, and since such  
 357 thermomechanical approaches usually rely on the assumption of an elastic be-  
 358 haviour for the solid phase with an appropriate potential, it is probably impos-  
 359 sible to generalize the conclusions obtained through thermomechanics outside  
 360 the assumed framework.

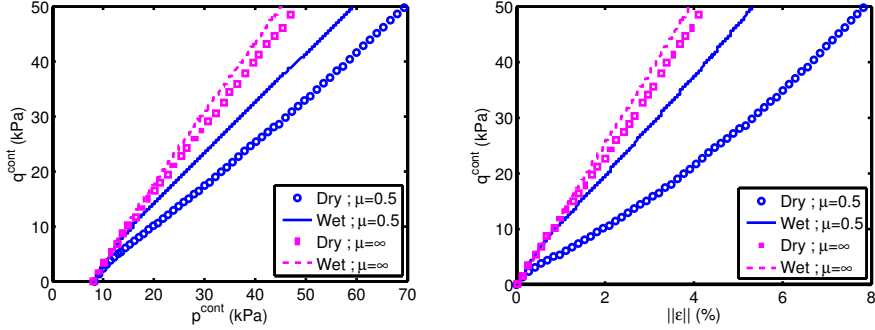


Figure 8: Influence of local friction  $\mu$  on the contact stress' effective nature for a loose packing along a contractant loading path ( $R = 5$ )

## 5. Comparison with Bishop's stress

### 5.1. Qualitative discussion

The present  $\mu$ UNSAT approach to effective stress is now compared with the commonly used effective stress expression as Bishop's stress  $\sigma^{Bish}$ :

$$\sigma' \stackrel{?}{=} \sigma^{Bish} = \Sigma - u_n \delta + u_c \chi \delta \quad (23)$$

Formally, significant differences appear between Bishop's equation (23) and the proposed  $\mu$ UNSAT equation (5). It is herein recalled that the  $\mu$ UNSAT equation includes a surface tension dependency in addition to that of capillary pressure, as well as the possibility of a non-spherical, microstructure-dependent, capillary stress contribution. Such features that characterize the microstructural details in triphasic materials go beyond the scope of Bishop's stress that relies on an average fluid pressure, being proportionnal to  $u_c$  and necessarily spherical. Since triphasic conditions by nature involve fluid-fluid interfaces and corresponding surface tension, the lack of  $\gamma^{nw}$  in Bishop's approach is questionable, as is the hypothesis of an averaged (isotropic) fluid pressure, while the wetted solid surfaces for instance experience capillary pressure along their normals only. Actually, the deviatoric nature of the capillary stresses has been repeatedly demonstrated in the pendular regime from modelling approaches [6, 26, 8, 24, 20], with possible variations in  $q^{cont}$  or  $q^{cap}$  independently of  $q$

379 during microstructural changes of the fluid phases, contrary to Bishop’s general  
 380 equality between  $q$  and  $q^{Bish}$ .

381 *5.2. Quantitative discussion*

382 In order to illustrate the inadequacy of Bishop’s stress to serve as an effective  
 383 stress in the pendular regime, other dry-wet comparisons are presented for the  
 384 dense packing along the two loading paths  $R \in \{1; 5\}$ , from initial states pre-  
 385 sented in Table 4. The present discussion actually narrows down to the classical  
 386 choice  $\chi = S_w$  for Bishop’s parameter, which can be continuously measured  
 387 during DEM simulations thanks to the complete description of the microstruc-  
 388 ture. As such, the stress response observed in dry conditions is now compared  
 389 to the Bishop’s stress response measured during triphasic conditions along the  
 390 same strain paths.

	Dry	Wet
Initial $p$ (kPa)	11.5	10
Imposed $u_c$ (kPa)	—	125
Initial $S_w$ (%)	—	0.85
Initial $n$ (-)	0.375	0.373
Initial $z_c$ (-)	6.41	6.52

Table 4: Tests data for the dry-wet comparison in terms of Bishop’s stress

391 Such loading paths  $R \in \{1; 5\}$  revealed a very good agreement of the  $\sigma^{cont-\epsilon}$   
 392 behaviours in both dry and wet conditions (Figs. 3 and 4). However, the wet  
 393 behaviour in terms of Bishop’s stress here significantly deviates from the dry be-  
 394 haviour (Fig. 9), clearly showing that Bishop’s stress is a much less appropriate  
 395 effective stress measure along these loading paths than the contact stress. In  
 396 addition to this degraded stress-strain effective character of Bishop’s stress, it  
 397 is also clear from the present comparison that Bishop’s stress is also inadequate  
 398 to describe the strength of wet materials from the dry plastic limit criterion,  
 399 which  $\sigma^{Bish}$  violates. The consideration of Bishop’s stress in an effective stress  
 400 approach with some dry shear strength criterion in practice would thus lead  
 401 to an overestimation of the risk of material failure in the pendular regime, in

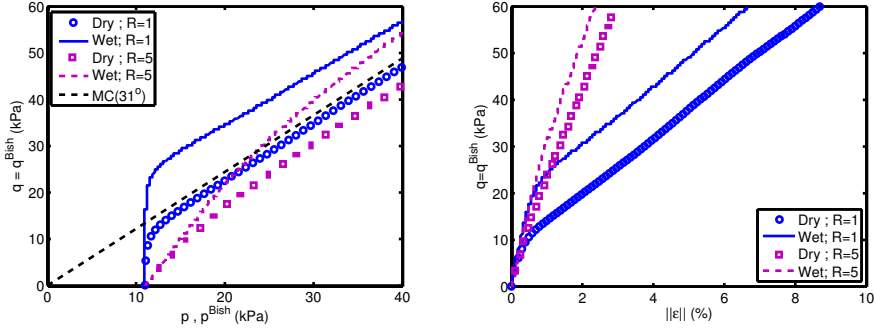


Figure 9: Bishop's or total stress responses along isochoric ( $R = 1$ ) and contractant ( $R = 5$ ) loading paths imposed on a dense packing

402 connection with an underestimation of capillary stresses already discussed in  
 403 [20, 24].

## 404 6. Conclusion

405 Micromechanical modelling approaches showed evidence of a single effective  
 406 stress variable that can be used together with dry constitutive relations  
 407 to describe the strains of idealized slightly polydisperse granular media in the  
 408 pendular regime. The appropriate variable is the contact stress whose direct  
 409 evaluation requires the prior knowledge of the contact force network. Using  
 410 the proposed  $\mu$ UNSAT expression, contact stresses can be alternatively calcu-  
 411 lated through measurements or estimations of the fluid phase microstructure  
 412 (interconnects), which are easier to determine than forces.

413 Unique contact stress-strain relationships have indeed been numerically demon-  
 414 strated along a variety of loading paths for both dry and wet (pendular regime)  
 415 conditions. This lends strong support to applying the effective stress designa-  
 416 tion to contact stress. However, the considered loading paths have to induce  
 417 small dissipation for the stress-strain effective stress approach to hold. Namely,  
 418 contractant loading paths and dense packings are well suited for the application  
 419 of the present  $\mu$ UNSAT approach to hold.

420 Previous experimental and phenomenological works by [4, 13] had restricted  
 421 the existence of a single stress-strain effective stress in triphasic media to the

422 elastic regime. This work based on microstructural analysis suggests a less  
423 restrictive condition by extending it to even the irreversible regime but with  
424 small dissipation.

425 There remain open questions as to whether new definitions of strain quan-  
426 tities could cast the presented results into an even more general framework.  
427 The present approach actually relies on observable strains or particle relative  
428 displacements that are due to both contact and capillary forces, through the  
429 classical DEM workflow (second Newton’s law). Alternatively, it could be at-  
430 tempted to define distinct, non-observable, strain components: first, a contact  
431 strain uniquely caused by contact forces, and second, a capillary strain uniquely  
432 due to capillary forces, with the combination of the two leading to the ob-  
433 servable strains herein considered. Such an alternative framework may lead to  
434 strictly unique constitutive relations between the contact stress and such a con-  
435 tact strain, and shed some light on the dissipation role through the yet to be  
436 defined link between contact strain and observable strain.

### 437 **Acknowledgements**

438 This work has been funded by the Natural Science and Engineering Research  
439 Council of Canada and Foundation Computer Modelling Group.

- 440 [1] K. Terzaghi, The shearing resistance of saturated soils and the angle be-  
441 tween the planes of shear, in: Proceedings of the 1st International con-  
442 ference on soil mechanics and foundation engineering, Vol. 1, Cambridge,  
443 1936, pp. 54–56.
- 444 [2] M. A. Biot, General theory of three-dimensional consolidation, *Journal of*  
445 *Applied Physics* 12 (2) (1941) 155–164. doi:10.1063/1.1712886.
- 446 [3] A. W. Bishop, G. E. Blight, Some aspects of effective stress in saturated  
447 and partly saturated soils, *Géotechnique* 13 (1963) 177–197.
- 448 [4] N. Khalili, F. Geiser, G. Blight, Effective stress in unsaturated soils: Review

- 449 with new evidence, *International Journal of Geomechanics* 4 (2) (2004) 115–  
450 126. [doi:10.1061/\(ASCE\)1532-3641\(2004\)4:2\(115\)](https://doi.org/10.1061/(ASCE)1532-3641(2004)4:2(115)).
- 451 [5] N. Lu, W. Likos, Suction stress characteristic curve for unsaturated soil,  
452 *Journal of Geotechnical and Geoenvironmental Engineering* 132 (2) (2006)  
453 131–142. [doi:10.1061/\(ASCE\)1090-0241\(2006\)132:2\(131\)](https://doi.org/10.1061/(ASCE)1090-0241(2006)132:2(131)).
- 454 [6] P.-Y. Hicher, C. Chang, A microstructural elastoplastic model for unsat-  
455 urated granular materials, *International Journal of Solids and Structures*  
456 44 (7-8) (2007) 2304 – 2323. [doi:10.1016/j.ijsolstr.2006.07.007](https://doi.org/10.1016/j.ijsolstr.2006.07.007).
- 457 [7] M. Nuth, L. Laloui, Effective stress concept in unsaturated soils: Clar-  
458 ification and validation of a unified framework, *International Journal for*  
459 *Numerical and Analytical Methods in Geomechanics* 32 (7) (2008) 771–801.  
460 [doi:10.1002/nag.645](https://doi.org/10.1002/nag.645).
- 461 [8] R. Wan, J. Duriez, F. Darve, A tensorial description of stresses in tripha-  
462 sic granular materials with interfaces, *Geomechanics for Energy and the*  
463 *Environment* 4 (2015) 73–87. [doi:10.1016/j.gete.2015.11.004](https://doi.org/10.1016/j.gete.2015.11.004).
- 464 [9] I. Cavarretta, I. Rocchi, M. Coop, A new interparticle friction apparatus  
465 for granular materials, *Canadian Geotechnical Journal* 48 (12) (2011) 1829–  
466 1840. [doi:10.1139/t11-077](https://doi.org/10.1139/t11-077).
- 467 [10] K. Senetakis, M. R. Coop, M. C. Todisco, The inter-particle coefficient of  
468 friction at the contacts of leighton buzzard sand quartz minerals, *Soils and*  
469 *Foundations* 53 (5) (2013) 746–755. [doi:10.1016/j.sandf.2013.08.012](https://doi.org/10.1016/j.sandf.2013.08.012).
- 470 [11] D. G. Fredlund, N. R. Morgenstern, R. A. Widger, The shear strength of  
471 unsaturated soils, *Canadian Geotechnical Journal* 15 (3) (1978) 313–321.  
472 [doi:10.1139/t78-029](https://doi.org/10.1139/t78-029).
- 473 [12] E. E. Alonso, A. Gens, A. Josa, A constitutive model for partially saturated  
474 soils, *Géotechnique* 40 (3) (1990) 405–430.



- 475 [13] E. Alonso, J.-M. Pereira, J. Vaunat, S. Olivella, A microstructurally based  
476 effective stress for unsaturated soils, *Géotechnique* 60 (2010) 913–925(12).  
477 [doi:10.1680/geot.8.P.002](https://doi.org/10.1680/geot.8.P.002).
- 478 [14] W. Baille, S. Tripathy, T. Schanz, Effective stress in clays of various min-  
479 eralogy, *Vadose Zone Journal* 13 (5). [doi:10.2136/vzj2013.06.0112](https://doi.org/10.2136/vzj2013.06.0112).
- 480 [15] J. Duriez, R. Wan, M. Pouragha, Partially saturated granular ma-  
481 terials: Insights from micro-mechanical modelling, in: *Proceedings*  
482 *of the 6th Biot Conference on Poromechanics, 2017*, pp. 441–448.  
483 [doi:10.1061/9780784480779.054](https://doi.org/10.1061/9780784480779.054).
- 484 [16] R. Hurley, E. Marteau, G. Ravichandran, J. E. Andrade, Extracting  
485 inter-particle forces in opaque granular materials: Beyond photoelastic-  
486 ity, *Journal of the Mechanics and Physics of Solids* 63 (2014) 154 – 166.  
487 [doi:10.1016/j.jmps.2013.09.013](https://doi.org/10.1016/j.jmps.2013.09.013).
- 488 [17] K. A. Culligan, D. Wildenschild, B. S. B. Christensen, W. G. Gray,  
489 M. L. Rivers, A. F. B. Tompson, Interfacial area measurements for unsat-  
490 urated flow through a porous medium, *Water Resources Research* 40 (12).  
491 [doi:10.1029/2004WR003278](https://doi.org/10.1029/2004WR003278).
- 492 [18] J.-F. Bruchon, J.-M. Pereira, M. Vandamme, N. Lenoir, P. Delage, X-ray  
493 microtomography characterisation of the changes in statistical homogene-  
494 ity of an unsaturated sand during imbibition, *Géotechnique Letters* 3 (2)  
495 (2013) 84–88. [doi:10.1680/geolett.13.00013](https://doi.org/10.1680/geolett.13.00013).
- 496 [19] J. Duriez, R. Wan, Contact angle mechanical influence for  
497 wet granular soils, *Acta Geotechnica* 12 (1) (2017) 67–83.  
498 [doi:10.1007/s11440-016-0500-6](https://doi.org/10.1007/s11440-016-0500-6).
- 499 [20] J. Duriez, M. Eghbalian, R. Wan, F. Darve, The micromechanical  
500 nature of stresses in triphasic granular media with interfaces,  
501 *Journal of the Mechanics and Physics of Solids* 99 (2017) 495–511.  
502 [doi:10.1016/j.jmps.2016.10.011](https://doi.org/10.1016/j.jmps.2016.10.011).

- 503 [21] M. E. Gurtin, A. I. Murdoch, A continuum theory of elastic material sur-  
504 faces, *Archive for Rational Mechanics and Analysis* 57 (4) (1975) 291–323.  
505 [doi:10.1007/BF00261375](https://doi.org/10.1007/BF00261375).
- 506 [22] X. Chateau, L. Dormieux, Homogenization of a non-saturated porous  
507 medium: Hill’s lemma and applications, *C. R. Acad. Sci. Paris, Série II*  
508 320 (1995) 627–634.
- 509 [23] W. G. Gray, B. A. Schrefler, Analysis of the solid phase stress tensor in mul-  
510 tiphase porous media, *International Journal for Numerical and Analytical*  
511 *Methods in Geomechanics* 31 (4) (2007) 541–581. [doi:10.1002/nag.541](https://doi.org/10.1002/nag.541).
- 512 [24] J. Duriez, R. Wan, Stress in wet granular media with interfaces via ho-  
513 mogenization and discrete element approaches, *Journal of Engineering Me-*  
514 *chanics* 142 (12). [doi:10.1061/\(ASCE\)EM.1943-7889.0001163](https://doi.org/10.1061/(ASCE)EM.1943-7889.0001163).
- 515 [25] V. Šmilauer, et al., *Yade Documentation 2<sup>nd</sup> ed*, The Yade Project, 2015.  
516 [doi:10.5281/zenodo.34073](https://doi.org/10.5281/zenodo.34073).  
517 URL <http://yade-dem.org/doc/>
- 518 [26] L. Scholtès, P.-Y. Hicher, F. Nicot, B. Chareyre, F. Darve, On the capillary  
519 stress tensor in wet granular materials, *International Journal for Numer-*  
520 *ical and Analytical Methods in Geomechanics* 33 (10) (2009) 1289–1313.  
521 [doi:10.1002/nag.767](https://doi.org/10.1002/nag.767).
- 522 [27] S. Herminghaus, Dynamics of wet granular matter, *Advances in Physics*  
523 54 (3) (2005) 221–261. [doi:10.1080/00018730500167855](https://doi.org/10.1080/00018730500167855).
- 524 [28] J. Duriez, R. Wan, Subtleties in discrete-element modelling of wet granular  
525 soils, *Géotechnique* 67 (4) (2017) 365–370. [doi:10.1680/jgeot.15.P.113](https://doi.org/10.1680/jgeot.15.P.113).
- 526 [29] I. F. Collins, The concept of stored plastic work or frozen elas-  
527 tic energy in soil mechanics, *Géotechnique* 55 (5) (2005) 373–382.  
528 [doi:10.1680/geot.2005.55.5.373](https://doi.org/10.1680/geot.2005.55.5.373).

- 529 [30] R. Puebla, A. Relaño, Irreversible processes without energy dissipation in  
530 an isolated Lipkin-Meshkov-Glick model, *Phys. Rev. E* 92 (2015) 012101.  
531 [doi:10.1103/PhysRevE.92.012101](https://doi.org/10.1103/PhysRevE.92.012101).
- 532 [31] M. Pouragha, R. Wan, Non-dissipative structural evolutions  
533 in granular materials within the small strain range, *International Journal of Solids and Structures* 110111 (2017) 94 – 105.  
534 [doi:10.1016/j.ijsolstr.2017.01.039](https://doi.org/10.1016/j.ijsolstr.2017.01.039).  
535
- 536 [32] A. Madeo, F. dell’Isola, F. Darve, A continuum model for deformable,  
537 second gradient porous media partially saturated with compressible fluids,  
538 *Journal of the Mechanics and Physics of Solids* 61 (11) (2013) 2196 – 2211.  
539 [doi:10.1016/j.jmps.2013.06.009](https://doi.org/10.1016/j.jmps.2013.06.009).
- 540 [33] E. Nikooee, G. Habibagahi, S. Hassanizadeh, A. Ghahramani, Effective  
541 stress in unsaturated soils: A thermodynamic approach based on the in-  
542 terfacial energy and hydromechanical coupling, *Transport in Porous Media*  
543 96 (2) (2013) 369–396. [doi:10.1007/s11242-012-0093-y](https://doi.org/10.1007/s11242-012-0093-y).